Crystal-melt interface stresses: Atomistic simulation calculations for a Lennard-Jones binary alloy, Stillinger-Weber Si, and embedded atom method Ni

C. A. Becker*

Department of Materials Science and Engineering, Northwestern University, Evanston, Illinois 60208, USA

J. J. Hoyt

Sandia National Laboratories, Albuquerque, New Mexico 87185, USA

D. Buta and M. Asta

Department of Chemical Engineering and Materials Science, University of California, Davis, California 95616, USA

Molecular-dynamics and Monte Carlo simulations have been used to compute the crystal-melt interface stress (f) in a model Lennard-Jones (LJ) binary alloy system, as well as for elemental Si and Ni modeled by many-body Stillinger-Weber and embedded-atom-method (EAM) potentials, respectively. For the LJ alloys the interface stress in the (100) orientation was found to be negative and the f vs composition behavior exhibits a slight negative deviation from linearity. For Stillinger-Weber Si, a positive interface stress was found for both (100) and (111) interfaces: $f_{100}=(380\pm30)$ mJ/m^2 and $f_{111}=(300\pm10)$ mJ/m^2. The Si (100) and (111) interface stresses are roughly 80 and 65% of the value of the interfacial free energy (γ), respectively. In EAM Ni we obtained $f_{100}=(22\pm74)$ mJ/m^2, which is an order of magnitude lower than γ. A qualitative explanation for the trends in f is discussed.

I. INTRODUCTION

For fluid-fluid or fluid-vacuum systems the reversible work required to form a unit area of interface is given by the interfacial free energy γ. An additional work term must be considered for interfaces where one or both phases is solid [1–3]. The quantity $Af_{ij}d\epsilon_{ij}$ represents the reversible work required to elastically stretch an interface of area A. The 2 $\times$ 2 tensor f_{ij} is known as the surface (or interface) stress and ϵ_{ij} is the surface strain. In a Lagrangian reference frame the interface stress is related to the interfacial free energy by the relation $f_{ij}=\gamma\delta_{ij}+\partial\gamma/\partial\epsilon_{ij}$ (where δ_{ij} is the Kronecker delta). For interfaces that display a threefold or higher axis of symmetry, the interface stress reduces to a scalar denoted as f.

In recent years several phenomena in which surface stress plays a pivotal role have been identified. Examples include surface reconstruction [4], the initial compressive stress during Volmer-Weber growth of thin films [5–8], warping and curling of free standing thin films [9], stabilization of small quantum-dot islands in heteroepitaxial growth [10–12], curvature and residual stress in multilayer films [7], plastic yielding [13] and structural phase transformations [14] in Au nanowires, nucleation in binary mixtures of hard spherical colloids [15], misfit dislocation generation in epitaxial thin films [16], and formation of stress-domain patterns on crystalline surfaces [17–20].

For crystal-vacuum and crystal-crystal interfaces, values of the interface stress for several systems have been reported. Atomistic simulations using first-principles techniques (e.g.,

Refs. [21–26]) and empirical potentials (e.g., Refs. [27–29]) have yielded the surface stress for a number of metal and insulating surfaces, whereas the interface stress has been measured from curvature experiments on various multilayer thin film systems [30–34]. In the case of crystal-liquid interfaces, however, very little is known. Using molecular dynamics (MD) simulation, Broughton and Gilmer [35] integrated the pressure profiles across the crystal-melt interface in the Lennard-Jones (LJ) system and found $f=-0.8\pm0.1$ (in reduced LJ units) for the (111) interface and $f=0.0\pm0.1$ for (100). In a detailed study of the structure and properties of the crystal-melt interface in the hard sphere system, Davidchack and Laird [36] reported the following values for the interface stress: $f_{111}=-0.71\pm0.13$ and $f_{100}=-0.17\pm0.06$. The results from these model systems are noteworthy for two reasons. First, in contrast to most computations of solid-vacuum surface stresses, f is negative. A negative stress implies the interface is in a state of compression and the crystal-melt system can lower its interfacial free energy by stretching the interface. Second, for the (111) crystal face the absolute value of f is quite large. For LJ the magnitude of f_{111} is greater than twice the interfacial free energy ($\gamma \approx 0.35$ [37–39]) and in the hard sphere system f_{111} is roughly 15% higher than γ [40]. The hard sphere and LJ systems are characterized by central force pair potentials and it is unclear whether the observed trends in f will hold for more realistic, many-body potentials.

In a recent MD study of a binary LJ alloy, Becker *et al.* [41] computed the orientationally averaged solid-liquid free energy as the temperature and composition were varied along the two-phase region of the lens-type phase diagram. They noted significant deviation from a linear interpolation of γ between the pure species. In addition the authors demonstrated that the variation with composition of the fourfold

*Present address: Metallurgy Division, Materials Science and Engineering Laboratory, National Institute of Standards and Technology, Gaithersburg, Maryland 20899.
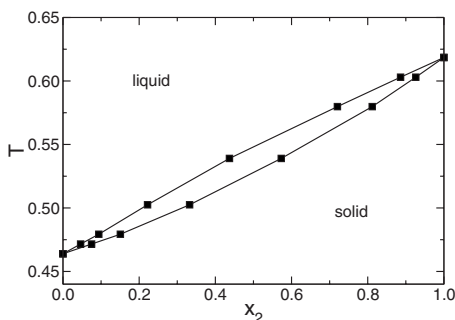
FIG. 1. The temperature-composition (x_2) phase diagram for the $\epsilon=0.75$, $\sigma=1$ LJ alloy.

and sixfold anisotropy parameters was strong enough to induce changes in dendrite tip orientations. Given the important effects of concentration on the interfacial free energy, it is of interest to investigate whether solute partitioning and the equilibrium concentration profile across the crystal-melt interface significantly affect the interface stress. Thus, the purpose of the present work is twofold. First, we employ atomistic simulations to examine the variation of f with alloying additions for the same LJ system studied by Becker *et al.* Second, we extend the interface stress computations to two additional interatomic potential schemes: the three-body potential developed by Stillinger and Weber [42] to model Si and a multibody embedded atom potential for pure Ni [43].

II. NUMERICAL PROCEDURES

An extensive survey of phase equilibria in binary LJ alloys has been performed by Hitchcock and Hall [44]. In their notation a given alloy is specified by two ratios: $\epsilon=\epsilon_{11}/\epsilon_{22}$ and $\sigma=\sigma_{11}/\sigma_{22}$ where ϵ_{ii} denotes the energy of interaction and σ_{ii} is the atomic size of species i. The cross-species interactions are given by the Lorentz-Berthelot mixing rules, that is, $\epsilon_{12}=\sqrt{\epsilon_{11}\epsilon_{22}}$ and $\sigma_{12}=(\sigma_{11}+\sigma_{22})/2$. In this work, as in the study of Ref. [41], we choose $\sigma=1$, meaning the two atomic species have the same bond length, and $\epsilon=0.75$.

In order to compare solid-liquid interface properties with previous studies, an interatomic potential truncation scheme introduced by Broughton and Gilmer [37] was used for all the LJ simulations. The phase diagram for the $\sigma=1, \epsilon=0.75$ LJ system is shown in Fig. 1, where T is the temperature in LJ units and x_2 is the concentration of species 2. As described in more detail in Ref. [45], the phase-diagram results were obtained employing thermodynamic integration methods based on the use of canonical and semi-grand-canonical Monte Carlo (MC) simulations [46]. Aside from a shift in the temperature scale arising from the use of a different potential-truncation scheme, the results plotted in Fig. 1 agree very well with those published for the same system by Hitchcock and Hall.

To compute interface stresses for the Lennard-Jones alloys use was made of Monte Carlo simulations for systems containing coexisting solid and liquid phases separated by (100)-oriented crystal-melt interfaces. The technique for equilibrating these solid-liquid systems followed closely the procedure discussed in detail in Ref. [45]. Specifically, simu-

lation cells were created from pure-solid samples measuring $7 \times 7 \times 22$ unit cells, where the latter dimension is the direction normal to the solid-liquid interface. Half of the system was melted and the dimensions and composition in the simulation cell adjusted to give rise to a system containing roughly equal volume fractions of solid and liquid phases with compositions and volumes given from the phase-diagram calculations at zero pressure. All systems were equilibrated in semi-grand-canonical MC simulations for at least 2×10^6 MC steps per atom, employing both atom-displacement and type-swap moves, with the imposed chemical-potential difference fixed at the coexistence values derived from the thermodynamic-integration calculations. In these equilibration runs the cross-sectional area parallel to the interfaces was held fixed at the value given by the zero-pressure lattice parameter of the crystal phase, while the periodic length normal to the interfaces was set to give the correct volumes (phase fractions) of solid and liquid. After equilibration, stress profiles and interface-stress values were derived from MC simulations lasting between 10^7 to 10^8 Monte Carlo steps, employing both atom-displacement and type-swap moves holding all periodic lengths fixed. For the purpose of deriving statistical uncertainties, these simulations were divided into between 90 and 190 independent subaverages. In the next section, results are presented showing stress profiles across the crystal-melt interfaces. These results were derived employing a filtering scheme as follows. Snapshots from the MC simulations were divided into bins parallel to the interface and the instantaneous stress components in each bin derived from the usual virial expressions; the resulting stress profiles were then "smoothed" using a Gaussian finite-impulse-response (FIR) filtering scheme as in Refs. [36,45], and the resulting smoothed profiles where then averaged over snapshots. The values of the filtering parameters employed in this analysis were the same as those used to compute density profiles in Ref. [45].

For elemental silicon, crystal-melt interface stress values were obtained by employing molecular-dynamics simulations based on the three-body potential developed by Stillinger and Weber [42]. Initially a bulk Si crystal was prepared and equilibrated at a temperature just below the known melting point for the potential [47–50] ($T_M=1678$ K) at zero pressure. A system with the same cross-sectional area A was melted, equilibrated at T_M and brought in contact with the crystal. The resulting two-phase cell was then equilibrated for 500 ps in the $NAP_{zz}T$ ensemble, where z refers to the direction normal to the crystal-melt boundary. In the final equilibration step, as in the coexistence technique described in Ref. [50], the system will approach the bulk melting temperature. Although the z dimension was allowed to vary (under zero imposed stress) during the equilibration, it was found to be convenient to periodically scale the normal dimension in order to achieve a very low value of the zz pressure. Statistics for the interface stress were collected every 100 MD time steps (1 time step=1 fs) in an NVE ensemble; statistically independent stress values, used to compute the uncertainties on f, were derived every 500 time steps. Two interface orientations for Si were investigated. The (111) cell contained a total of 59250 atoms and the (100) geometry consisted of 72 900 atoms.

Molecular-dynamics simulations of pure Ni utilized the embedded atom method interatomic potential developed by Foiles, Baskes, and Daw [43] for which the melting temperature (1710 K) is well established [51]. A cell dimension of $20 \times 20 \times 40$ unit cells (64 000 atoms) with a (100) orientation was employed. After melting one half of the simulation cell at an elevated temperature, the system was equilibrated using an $NAP_{zz}T$ ensemble. Statistics for the interface stress were collected every 20 ps (time step=2 fs) in an NVE ensemble.

III. RESULTS

In calculations of the surface stress (i.e., the surface tension) for liquid-vapor surfaces the following expression is commonly employed (see e.g., Ref. [52]):

$$f = \frac{1}{2} \int_0^{L_z} [P_\perp(z) - P_\parallel(z)] dz, \tag{1}$$

where $P_\perp$ and $P_\parallel$ are the normal and transverse components of the virial pressure, the integral is performed over the entire length of the system L_z, and the factor of 1/2 accounts for the presence of two surfaces in periodic simulation cells. For interface simulations containing at least one crystalline phase, Eq. (1) is not strictly valid due to the nonhydrostatic nature of the stress tensor in a crystal. Nevertheless, Eq. (1) can be used to derive an accurate estimate of f provided that the so-called crystal stress [36] is very small. The crystal stress is obtained by integrating $[P_\perp(z) - P_\parallel(z)]$ over the bulk-crystalline region of the simulation cell, and it represents the residual nonhydrostatic component of the stress remaining in the solid after equilibration of the two-phase system. [We note that for each of the systems considered in this work care was taken to equilibrate the simulations to achieve as low a value of the normal stress as possible, and, thus Eq. (1) reduces in this case to an integral of $-P_\parallel(z)$ normal to the interfaces.]

The upper panel of Fig. 2 shows the quantity $P_\perp - P_\parallel$ in reduced units of $\epsilon_{22}/\sigma_{22}^3$ versus the z position normal to the interface for the LJ binary system. Six temperatures, corresponding to the six alloy phase boundaries in Fig. 1, are depicted. The two large negative spikes in the data occur at the positions of the two crystal-melt interfaces and the area contained within these peaks represents the interface stress. The relatively flat portions of the $P_\perp - P_\parallel$ curves located in the middle of the system, i.e., in the vicinity of $z=20$, correspond to the residual crystal stress referred to above. Values of the crystal stress are small relative to the sharp peaks at the interfaces; nevertheless, in order to observe subtle changes in f with composition, the crystal stress contribution has been subtracted in the results to follow. Finally, in the outside portions of the system, which represent the liquid phase, the pressure difference $P_\perp - P_\parallel$ is nearly zero as expected.

The bottom panel of Fig. 2 plots $P_\perp$ ($=P_{zz}$) versus z position. In a well equilibrated MD system the normal component of the pressure should be zero, and as is shown in Fig. 2 the normal pressure is indeed quite low. We do, however,
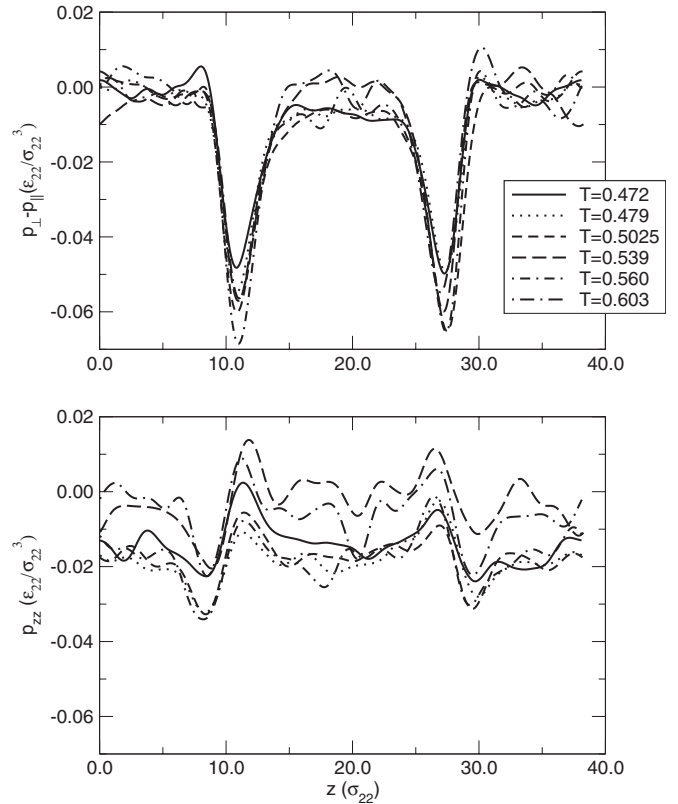

FIG. 2. Top: the normal pressure minus the transverse pressure in units of $\epsilon_{22}/\sigma_{22}^3$ vs the distance normal to the crystal-melt interface. Data for six temperatures, corresponding to the six compositions shown in Fig. 1, are shown. The large negative peaks occur at the positions of the two interfaces in the periodic cell. Bottom: the normal pressure P_{zz} vs position along the z direction.

observe a nonuniform behavior of P_{zz} in the vicinity of the interface for all temperatures. A similar trend is apparent in the stress profiles reported for hard spheres by Davidchack and Laird [36], although the nonuniform nature of the P_{zz} profiles is less pronounced in their results, relative to the present work. The nonconstant normal pressure likely arises due to atomic structure changes in the vicinity of the interface, and may be somewhat amplified by the choice of filtering parameters which were not optimized specifically to smooth these profiles. Overall, the amplitudes of the variations in P_{zz} are relatively small and the integrals of these profiles over z are nearly zero.

Figure 3 shows the (100) interface stress in units of $\epsilon_{22}/\sigma_{22}^2$ versus the alloy composition x_2, where the error bars represent estimated standard statistical uncertainties. The dashed line in the figure is constructed by assuming the interface stress is a composition-weighted average of the two pure systems (the slope of the line is fixed by the parameter $\epsilon = \epsilon_{11}/\epsilon_{22} = 0.75$). The data of Fig. 3 suggest a negative deviation from the ideal mixing line; however, the magnitude of the deviation is difficult to assess precisely due to the considerable scatter and relatively large statistical uncertainties associated with the simulation data. It is interesting to note, however, that the interfacial free energy for this LJ binary alloy exhibits the opposite trend, i.e., a positive deviation from linearity. For the four temperatures where both
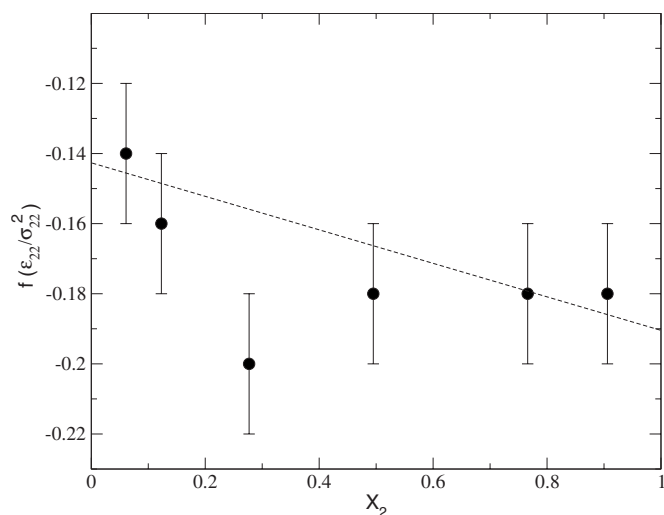
FIG. 3. Crystal-melt interface stress for the $\epsilon=0.75$, $\sigma=1$ LJ alloy vs the composition x_2. The dashed line represents a linear interpolation of the stresses for the two pure components.

the interface stress f and the interfacial free energy γ (Ref. [41]) were calculated for the (100) interfaces (T=0.479, 0.5025, 0.539, and 0.603), the magnitudes of the ratio of f/γ are in the range of 0.24 to 0.53.

It is noteworthy that the dashed line in Fig. 3 leads to a prediction for the value of f_{100} for the pure element (given by $x_2=1$) which is approximately equal to -0.19 in LJ units. Due to the fact that this estimate is based on an extroplation of data that shows a clear deviation from linearity, the uncertainties in this value are relatively high. However, it is clear that the data in Fig. 3 suggests a pure-element value for f_{100} which is considerably larger in magnitude than the estimate of $f_{100}=0.0\pm0.1$ reported by Broughton and Gilmer [35]. This apparent discrepancy may reflect higher than reported uncertainties in their calculated stresses due the smaller systems and more limited statistics available to the authors in this early work. We note that the sign and appreciable magnitude of f_{100} estimated from the previous calculations is qualitatively similar to the results for the hard-sphere system [36]. Using the current estimate of $f_{100}\approx-0.19$, the magnitudes of f/γ for the pure elements are consistent with those of the alloys reported in the previous paragraph.

As mentioned in the Introduction, a striking feature of the crystal-melt interface stresses in the LJ and hard-sphere systems is the large negative values reported, particularly for (111)-oriented interfaces. A possible, qualitative explanation for the $f<0$ result is as follows. In the LJ and hard-sphere models the density of the liquid is less than that of the crystal, meaning the average interatomic spacing is larger in the liquid phase. When the liquid with a smaller packing fraction is placed in contact with a more closely packed solid a compressive stress ($f<0$) at the interface results as the less dense liquid tends to stretch the interface. This simplistic picture of the interface stress is supported by the fact that the more close-packed (111) interface stress is more negative than f_{100} for both LJ and hard-sphere systems [35,36].

To further test this qualitative explanation for the observed behavior of f in the LJ system, consider the case of

Si. Here the density in the liquid is higher than that of the crystal and thus one would expect the sign of f to be reversed. For the Stillinger-Weber system we obtain a (100) crystal-melt interface stress of $f_{100}=(380\pm30)$ mJ/m^2, whereas for the (111) orientation we find $f_{111}=(300\pm10)$ mJ/m^2. These values were not corrected for the crystal stress, the contribution of which was estimated to be roughly equivalent to the uncertainty, i.e., ≈10 mJ/m^2. It is instructive to compare the interface stress with the interfacial free energy. Maximum undercooling nucleation experiments have produced three estimates of γ for Si: Stiffler *et al.* [53] reported a value of $\gamma=340$ mJ/m^2 at a temperature of $T=1180$ K, Shao and Spaepen [54] found $\gamma=355$ mJ/m^2 at 1335 K and Liu *et al.* [55] obtained $\gamma=400$ mJ/m^2 at 1335 K. Ujihara *et al.* [56] proposed a model for the temperature dependence of the solid-liquid interfacial free energy that agrees well with the experimental results; the authors find $\gamma=463$ mJ/m^2 at the melting point. Thus, the relative magnitudes of the (100) interface stress and γ for Si are similar to those found in LJ, but positive. Also, the (111) interface stress for Si is positive, but the ratio f/γ is smaller in magnitude than the LJ result. However, the comparison in the case of (111) is complicated by the fact that in Si the (111) crystal-melt interface is faceted rather than rough [47].

The LJ interaction energy is of the pair-potential type, meaning the energy of an atom depends only on the distance of separation of all of its neighbors. In order to capture the tetrahedral bonding of the diamond cubic structure, the Stillinger-Weber potential employs a three-body term that depends on the angles and interatomic distances in triplets of Si atoms. In contrast, the embedded atom method model of interatomic bonding in a metallic system incorporates multibody effects through a term that depends nonlinearly on the local electron density. For many bulk and surface properties in metals the multibody form of the EAM represents a significant improvement over pair-potential schemes [57]. For example, the correct sign of the change in surface interlayer spacing for several late transition metals is captured using the EAM formalism [58]. In light of the qualitative discussion of f presented above, it is of interest to predict how the EAM model will alter the sign and magnitude of the crystal-melt interface stress. In pure Ni the density of the liquid is less than the solid and, from the point of view of the qualitative argument offered above it might be expected that as in the case of the LJ system, the crystal-melt interface will be able to lower its free energy by stretching. On the other hand, the EAM form for the interatomic potential is known to give rise to shorter, more stiff, bonds in lower-density configurations [57]. Thus, from this standpoint it might be expected that the EAM multibody terms give rise to a tensile component to the interface stress. If these competing compressive and tensile effects are of comparable magnitude, a very low value of f may result. Indeed, for EAM Ni in the (100) orientation we find $f=(22\pm74)$ mJ/m^2, a value that is over a factor of ten lower than the interfacial free energy ($\gamma=285$ mJ/m^2) computed from the capillary fluctuation method [51,59].

IV. DISCUSSION

As noted by Spaepen [7] the interface stress in multilayer thin films is usually large and negative. For example, in

(111) textured Ag/Cu films $f=(-3190\pm430)$ mJ/m^2 [31] and for (111) textured Ag/Ni films two values of f have been reported: $f=(-2270\pm670)$ mJ/m^2 [30] and $f=(-2240\pm210)$ mJ/m^2 [32]. However, an EAM atomistic study by Gumbsch and Daw [28] has found a positive $f=320$ mJ/m^2 for both systems. Given the sensitivity of the magnitude and sign of the interface stress on the details of the interatomic potential as found in this study, the discrepancy between experiment and the EAM result is perhaps not surprising. In particular, the Gumbsch and Daw study employed an alloy interaction that was derived from a mixing rule [43] for the repulsive part of the pure component potentials. It would be of interest to repeat the calculation of interface stress in these systems using an interatomic potential that is fit directly to alloy properties.

Jiang *et al.* [60] have proposed a phenomenological model for the interface stress by examining the elastic strain imposed on a small solid immersed in a fluid of the same composition and defining a small particle diameter D_0 where the sphere becomes indistinguishable from the fluid. In terms of an atomic diameter h the quantity D_0 for a sphere can be approximated as $D_0=3h$. The final expression obtained by the authors is given by

$$f = \pm[(3\gamma_0 D_0)/(8\kappa)]^{1/2}, \qquad (2)$$

where γ_0 refers to the solid-liquid interfacial free energy for an infinitely large particle and κ is the compressibility of the solid. Although a negative f is predicted for the case of multilayer films, consistent with experimental findings, the interface stress appears to be positive for crystal-melt systems. Therefore, the model is unable to explain the $f<0$ results found for both the hard sphere and LJ systems. In addition, Eq. (2) overestimates the magnitude of the interface stress. The authors note that the predicted f is roughly one order of magnitude higher than γ, but the results for Stillinger-Weber Si show that f is at most 0.82γ whereas the MD prediction for EAM Ni demonstrates that the interface stress is an order of magnitude *less* than γ, and the prediction for Lennard-Jones depends on orientation and composition with f no more than approximately twice γ [35]. Finally, Jiang *et al.* apply their model to the case of solid-vacuum interfaces and obtain reasonable agreement with computed values of f. However, direct application of the crystal-melt model in Eq. (2) to the case of crystal-vacuum surfaces relies on the assumption that the fluid has no effect on the surface strain of solids. The MD results suggest that the fluid plays a dominant role in setting the strain at the crystal surface and we propose that the density difference between solid and liquid gives rise to the negative f values seen in pair potential models.

For nonzero values of f, it has been shown [61] from a continuum elasticity analysis of an unstressed crystal that the interface is morphologically unstable for fluctuations with wavelengths below some critical size. However, as pointed out by Grilhe, if the interface stress is of the same order or smaller than the interfacial free energy, as is observed here, the critical wavelength becomes on the order of a few atomic spacings and at this small length scale the validity of the continuum approximation breaks down. In the capillary fluctuation analysis of the LJ system [41] we have observed no contribution of the roughness due to stretching of the interface and we conclude that the interface stress contribution to the interface morphology must be small relative to capillary fluctuations.

V. CONCLUSIONS

The crystal-melt interface stress in the (100) orientation is found to be negative for a series of LJ alloys. In addition, the f vs x_2 behavior exhibits a slight negative deviation from a linear extrapolation of the two pure systems. The LJ results stand in stark contrast to the interface stresses computed for Stillinger-Weber Si. In Si, f_{100} and f_{111}, when normalized by the interfacial free energy γ, are similar in magnitude to the LJ alloy system, but are positive. We propose that the change in the sign of f can be qualitatively understood by the different sign associated with the density change on melting in the LJ versus Stillinger-Weber Si systems. For LJ, with a lower density liquid, the fluid phase imparts a tensile strain on the crystal ($f<0$), whereas in Si the liquid density is higher than that of the crystal and the opposite trend is observed. In EAM Ni, the tendency of the less-dense liquid to stretch the crystal surface is offset by the increased bond strength resulting from the density dependent interaction energy. Hence the (100) interface stress in Ni is over an order of magnitude less than γ.

ACKNOWLEDGMENTS

[1] J. W. Gibbs, *Scientific Papers, Vol. 1: Thermodynamics* (Dover Publications, New York, 1961).

[2] J. W. Cahn, Acta Metall. **28**, 1333 (1980).

[3] R. C. Cammarata, Prog. Surf. Sci. **46**, 1 (1994).

[4] H. Ibach, Surf. Sci. Rep. **29**, 195 (1997), and references therein.

[5] R. C. Cammarata, T. M. Trimble, and D. J. Srolovitz, J. Mater. Res. **15**, 2468 (2000).

[6] J. A. Floro, E. Chason, R. C. Cammarata, and D. J. Srolovitz, MRS Bull. **27**, 19 (2002).

[7] F. Spaepen, Acta Mater. **48**, 31 (2000).

[8] F. Spaepen, J. Mech. Phys. Solids **44**, 675 (1996).

[9] K. G. Kornev and D. J. Srolovitz, Appl. Phys. Lett. **85**, 2487 (2004).

[10] O. E. Shklyaev, M. J. Beck, M. Asta, M. J. Miksis, and P. W. Voorhees, Phys. Rev. Lett. **94**, 176102 (2005).

[11] G.-H. Lu and F. Liu, Phys. Rev. Lett. **94**, 176103 (2005).

[12] P. Kratzer, Q. K. K. Liu, P. Acosta-Diaz, C. Manzano, G. Costantini, R. Songmuang, A. Rastelli, O. G. Schmidt, and K. Kern, Phys. Rev. B **73**, 205347 (2006).

[13] J. K. Diao, K. Gall, M. L. Dunn, and J. A. Zimmerman, Acta Mater. **54**, 643 (2006).

[14] J. K. Diao, K. Gall, and M. L. Dunn, Nat. Mater. **2**, 656 (2003).

[15] A. Cacciuto, S. Auer, and D. Frenkel, Phys. Rev. Lett. **93**, 166105 (2004).

[16] R. C. Cammarata, K. Sieradzki, and F. Spaepen, J. Appl. Phys. **87**, 1227 (2000).

[17] V. I. Marchenko, JETP Lett. **33**, 381 (1981).

[18] O. L. Alerhand, D. Vanderbilt, R. D. Meade, and J. D. Joannopoulos, Phys. Rev. Lett. **61**, 1973 (1988).

[19] J. B. Hannon, F. J. Meyer zu Heringdorf, J. Tersoff, and R. M. Tromp, Phys. Rev. Lett. **86**, 4871 (2001).

[20] R. van Gastel, N. C. Bartelt, P. J. Feibelman, F. Leonard, and G. L. Kellogg, Phys. Rev. B **70**, 245413 (2004).

[21] R. J. Needs, Phys. Rev. Lett. **58**, 53 (1987).

[22] R. J. Needs, M. J. Godfrey, and M. Mansfield, Surf. Sci. **242**, 215 (1991).

[23] D. Vanderbilt, Phys. Rev. Lett. **59**, 1456 (1987).

[24] M. C. Payne, N. Roberts, R. J. Needs, M. Needels, and J. D. Joannopoulos, Surf. Sci. **211**, 1 (1989).

[25] V. Fiorentini, M. Methfessel, and M. Scheffler, Phys. Rev. Lett. **71**, 1051 (1993).

[26] P. J. Feibelman, Phys. Rev. B **51**, 17867 (1995).

[27] G. J. Ackland and M. W. Finnis, Philos. Mag. A **54**, 301 (1986).

[28] P. Gumbsch and M. S. Daw, Phys. Rev. B **44**, 3934 (1991).

[29] V. B. Shenoy, Phys. Rev. B **71**, 094104 (2005).

[30] J. A. Ruud, A. Witvrouw, and F. Spaepen, J. Appl. Phys. **74**, 2517 (1993).

[31] S. Berger and F. Spaepen, Nanostruct. Mater. **6**, 201 (1995).

[32] K. O. Schweitz, H. Geisler, J. Chevalier, J. Bottiger, and R. Feidenhans'l, Mater. Res. Soc. Symp. Proc. **505**, 559 (1998).

[33] D. Josell, J. E. Bonevich, I. Shao, and R. C. Cammarata, J. Mater. Res. **14**, 4358 (1999).

[34] C. Friesen, N. Dimitrov, R. C. Cammarata, and K. Sieradzki, Langmuir **17**, 807 (2001).

[35] J. Q. Broughton and G. H. Gilmer, Acta Metall. **31**, 845

[36] R. L. Davidchack and B. B. Laird, J. Chem. Phys. **108**, 9452 (1998).

(1983).

[37] J. Q. Broughton and G. H. Gilmer, J. Chem. Phys. **84**, 5759 (1986).

[38] R. L. Davidchack and B. B. Laird, J. Chem. Phys. **118**, 7651 (2003).

[39] J. R. Morris and X. Song, J. Chem. Phys. **119**, 3920 (2003).

[40] R. L. Davidchack and B. B. Laird, Phys. Rev. Lett. **85**, 4751 (2000).

[41] C. A. Becker, D. Olmsted, M. Asta, J. J. Hoyt, and S. M. Foiles, Phys. Rev. Lett. **98**, 125701 (2007).

[42] F. H. Stillinger and T. A. Weber, Phys. Rev. B **31**, 5262 (1985).

[43] S. M. Foiles, M. I. Baskes, and M. S. Daw, Phys. Rev. B **33**, 7983 (1986).

[44] M. R. Hitchcock and C. K. Hall, J. Chem. Phys. **110**, 11433 (1999).

[45] C. A. Becker, M. Asta, J. J. Hoyt, and S. M. Foiles, J. Chem. Phys. **124**, 164708 (2006).

[46] H. Ramalingam, M. Asta, A. van de Walle, and J. J. Hoyt, Interface Sci. **10**, 149 (2002).

[47] U. Landman, W. D. Luedtke, R. N. Barnett, C. L. Cleveland, M. W. Ribarsky, E. Arnold, S. Ramesh, H. Baumgart, A. Martinez, and B. Khan, Phys. Rev. Lett. **56**, 155 (1986).

[48] D. K. Chokappa, S. J. Cook, and P. Clancy, Phys. Rev. B **39**, 10075 (1989).

[49] J. Q. Broughton and X. P. Li, Phys. Rev. B **35**, 9120 (1987).

[50] S. Yoo, X. C. Zeng, and J. R. Morris, J. Chem. Phys. **120**, 1654 (2004).

[51] J. J. Hoyt, M. Asta, and A. Karma, Mater. Sci. Eng., R. **41**, 121 (2003).

[52] S. W. Sides, G. S. Grest, and Martin-D. Lacasse, Phys. Rev. E **60**, 6708 (1999).

[53] S. R. Stiffler, M. O. Thompson, and P. S. Peercy, Phys. Rev. Lett. **60**, 2519 (1988).

[54] Y. Shao and F. Spaepen, J. Appl. Phys. **79**, 2981 (1996).

[55] R. P. Liu, T. Volkmann, and D. M. Herlach, Acta Mater. **49**, 439 (2001).

[56] T. Ujihara, G. Sazaki, K. Fujiwara, N. Usami, and K. Nakajima, J. Appl. Phys. **90**, 750 (2001).

[57] A. E. Carlsson, Solid State Phys. **43**, 1 (1990).

[58] M. S. Daw, S. M. Foiles, and M. I. Baskes, Mater. Sci. Rep. **9**, 251 (1993).

[59] J. J. Hoyt, M. Asta, and A. Karma, Phys. Rev. Lett. **86**, 5530 (2001).

[60] Q. Jiang, L. H. Liang, and D. S. Zhao, J. Phys. Chem. B **105**, 6275 (2001).

[61] J. Grilhe, Acta Metall. Mater. **41**, 909 (1993).